HIGH-VELOCITY IMPACT DAMAGE PROGRESS IN CFRP LAMINATES

E. Oka[1], K. Ogi[1]*, A. Yoshimura[2], T. Okabe[3]
[1] Graduate School of Science and Engineering, Ehime University, Matsuyama, Japan
[2] Japan Aerospace Exploration Agency, Mitaka, Japan
[3] Graduate School of Engineering, Tohoku University, Sendai, Japan

* Corresponding author(ogi.keiji.mu@ehime-u.ac.jp)

Keywords: *CFRP, High-velocity impact, Delamination, Matrix cracking, FEM*

1 Introduction

Since CFRP fan blades and a CFRP fan case have already been applied to a recently-developed turbo fan engine such as GEnx, foreign object damage (FOD) is a critical problem. Hence, it is essential to facilitate a FOD process model for the durability of the CFRP fan system. However, the detailed process of FOD at around a sound velocity has not been clarified thoroughly because it is very complicated. Hence, the primary purpose of the present study is to characterize the high-velocity impact damage progress in CFRP laminates. The secondary aim is to investigate the effect of mechanical properties on high-velocity impact damage progress.
First, the surface and internal damages of CFRP plates impacted at velocities of 200 and 400 m/s were observed by using optical microscopy together with radiography. Next, dynamic finite element analysis (FEA) was performed to simulate the damage process. Cohesive elements were introduced to express the delamination and splitting cracks while the maximum stress fracture criteria were employed to express the intralaminar failure. The simulation results were then compared with the experiment results to verify the reasonability of the analysis. Finally, effects of lamina strength and interlaminar fracture toughness on damage evolution were investigated through parametric study.

2 Experimental Procedures

High speed impact tests were performed using an impact testing machine with an electroheat gun. A steel ball with a diameter of 1.5 mm (14.2 mg) was used as a projectile. A projectile set in a sabot was accelerated by high-temperature and high-pressure metal plasma, which is produced by melting and evaporation of an aluminum foil subjected to high-voltage pulse current. The CFRP (carbon/epoxy) unidirectional (UD, $[0°_{16}]$) and cross-ply (CP, $[0°/90°]_{4S}$) laminates (55 mm x 55 mm x 1.6 mm) were employed as targets. The detail of the test was described in the literature [1]. The target specimens 55 mm square and 1.6 mm thick was rigidly fixed along it four sides by a square frame jig with inner width of 50 mm. Thus, this support allows bending deformation in the target during impact load.
The surface and the internal damages of the specimens were observed by using optical microscopy and radiography for two impact velocities, $v = 200$ and 400 m/s.

3 Numerical Simulation

Dynamic FEA was performed using a commercial FE software (Abaqus, MSC). A quarter three-dimensional model was adopted for symmetry as shown in Fig. 1. The 8-node solid elements were employed in addition to the 8-node cohesive elements, that were inserted at all the interlayers. Additionally, the cohesive elements were also introduced on the front and back surfaces for reproducing splitting cracks. Additional user subroutine programs for the maximum stress failure criteria was applied to the intralaminar failure. The relation between the traction force and relative displacement for cohesive elements was assumed to be bilinear [2]. For the onset of failure in cohesive elements, the following quadratic criterion was employed:

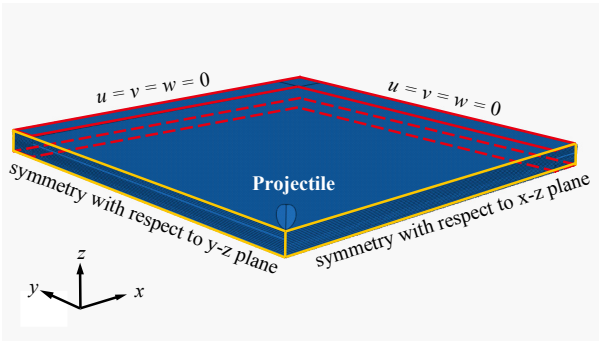

Fig.1. Model for finite element analysis.

$$\left(\frac{\langle t_{\mathrm{I}}\rangle}{t_{\mathrm{I}}^{0}}\right)^{2}+\left(\frac{t_{\mathrm{II}}}{t_{\mathrm{II}}^{0}}\right)^{2}+\left(\frac{t_{\mathrm{III}}}{t_{\mathrm{III}}^{0}}\right)^{2}=1 \qquad (1)$$

where t_i denotes the traction (stress), t_i^0 the strength, and the subscripts modes I, II, and III. In contrast, for development of failure, the following mixed-mode criterion was adopted:

$$G_{\mathrm{I}}^{\mathrm{C}}+\left(G_{\mathrm{II}}^{\mathrm{C}}-G_{\mathrm{I}}^{\mathrm{C}}\right)\left(\frac{G_{\mathrm{II}}+G_{\mathrm{III}}}{G_{\mathrm{T}}}\right)^{\eta}=G_{\mathrm{T}} \qquad (2)$$

with $G_{\mathrm{T}}=G_{\mathrm{I}}+G_{\mathrm{II}}+G_{\mathrm{III}}$, where G_i denotes the energy release rate, G_i^{C} the interlaminar fracture toughness, and η a fitting parameter ($\eta=1.5$). The material constants in the literature [3] were used and listed in Tables 1 to 3. Additionally, the lamina tensile and compressive strengths, denoted by $\sigma_{1\mathrm{T}}$ and $\sigma_{1\mathrm{C}}$, and the interlaminar fracture toughness G_i^{C} were varied as parameters to investigate their effects on damage progress. The combinations of $\sigma_{1\mathrm{T}}$, $\sigma_{1\mathrm{C}}$, and G_i^{C} are presented in Table 4.

4 Results and Discussion

Figure 2 presents the damage states on the front and back surfaces in the UD laminate. Some splitting cracks in the fiber direction (arrow A) were propagating from a crater on the front surface. In contrast, only splitting cracks (arrow B) were generated on the back surface. The surface failure mode makes little difference between UD and CP laminates.

Figure 3 depicts the simulated matrix-damaged region on both surfaces of the UD laminate. The

Table 1 Material properties of CFRP and steel.

	CFRP		Steel
Young's modulus (GPa)	E_1	135	Assuming a rigid body
	$E_2=E_3$	7.8	
Shear modulus (GPa)	$G_{12}=G_{13}$	4.4	
	G_{23}	2.7	
Poisson's ratio	$\nu_{12}=\nu_{13}$	0.34	
	ν_{23}	0.4	
Density (g/cm^3)	1.6		7.8

Table 2 Strength in each direction of a UD laminate.

Direction	Strength (MPa)
Longitudinal (1) / Tension	2200
Longitudinal (1) / Compression	1400
Transverse (2) / Tension	65
Transverse (2) / Compression	1000
Thickness (3) / Compression	1000
In-plane shear (1-2)	98
Out-of-plane shear (1-3, 2-3)	98

Table 3 Strength and fracture toughness of cohesive elements.

	Delamination	Splitting
t_{I}^0 MPa	30	75
t_{II}^0, t_{III}^0 MPa	60	100
$G_{\mathrm{I}}^{\mathrm{C}}$ J/m^2	200	150
$G_{\mathrm{II}}^{\mathrm{C}}$, $G_{\mathrm{III}}^{\mathrm{C}}$ J/m^2	600	300

Table 4 Combinations of $\sigma_{1\mathrm{T}}$, $\sigma_{1\mathrm{C}}$, and G_i^{C} used in the parametric study.

No.	$\sigma_{1\mathrm{T}}$ (MPa)	$\sigma_{1\mathrm{C}}$ (MPa)	$G_{\mathrm{I}}^{\mathrm{C}}$ (J/m^2)	$G_{\mathrm{II}}^{\mathrm{C}}$ (J/m^2)	$G_{\mathrm{III}}^{\mathrm{C}}$ (J/m^2)
1	2200	1400	200	600	600
2	1100	700	200	600	600
3	3300	2100	200	600	600
4	2200	1400	100	300	300
5	2200	1400	400	1200	1200

damage states including a crater and splitting cracks are well reproduced in the analysis.

Figure 4 shows the cross-sectional views of the UD and CD laminates for v = 400 m/s. A deep crater, delamination, and breakage of several laminae are observed in both laminates. Cone cracking is observed only in the UD laminate while the opening displacement of the delamination is larger in the CP laminate. It should be noted that the projectile perforated only through the UD laminate at this impact velocity. Simulated internal damage states that correspond to Fig. 4 are depicted in Fig. 5. Damage states including crater depth and delamination are reasonably reproduced in the analysis, although cone cracking is not reproduced.

Figure 6 shows the soft X-ray photos of the UD and CP laminates after impact. The delamination in the UD laminate extends in the fiber direction, which results in a galaxy-shaped delamination. This delamination is narrow because it propagates along the splitting cracks on the surfaces. In contrast, the circle-shaped delamination was generated in the CP laminate. This shape results from the superposition of two peanut-shaped delaminations. Figure 7 demonstrates the simulated delamination in the UD

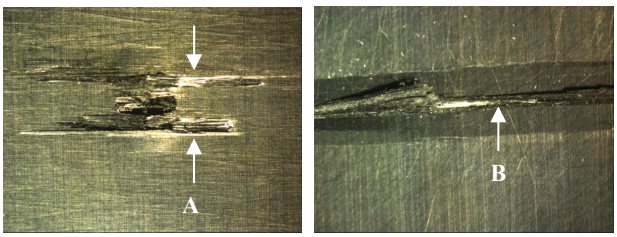

(a) Front (b) Back

Fig.2. Observed damage states on the (a) front and (b) back surfaces of the UD laminates after impact (v = 400 m/s).

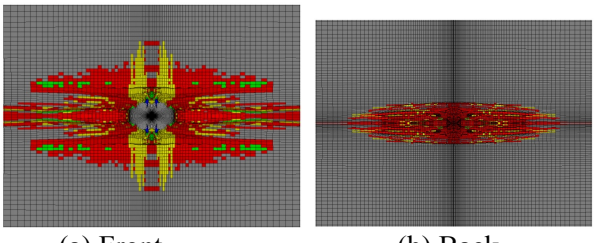

(a) Front (b) Back

Fig.3. Simulated surface damage states of UD laminates after impact (v = 400 m/s).

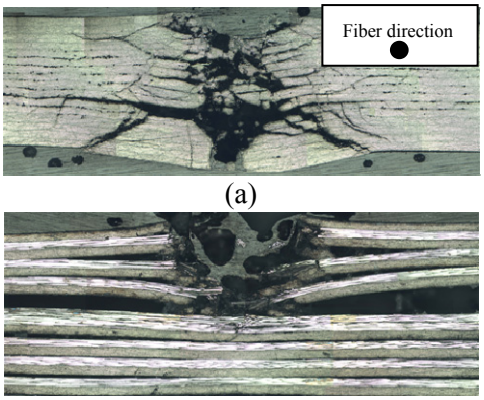

(a)

(b)

Fig. 4 Cross-sectional views of the (a) UD and (b) CP laminates for v = 400 m/s.

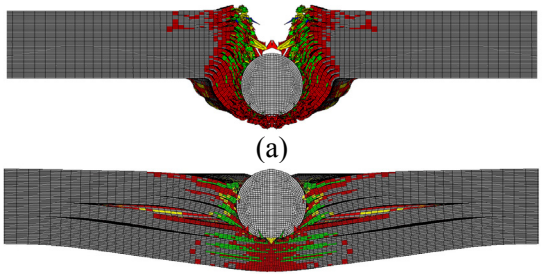

(a)

(b)

Fig. 5 Simulated internal damage states of the (a) UD and (b) CP laminates for v = 400 m/s.

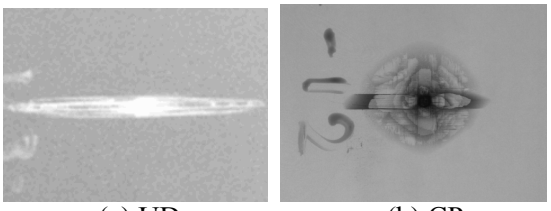

(a) UD (b) CP

Fig.6. Soft X-ray photos of the internal damage states in the UD and CP laminates (v = 400 m/s).

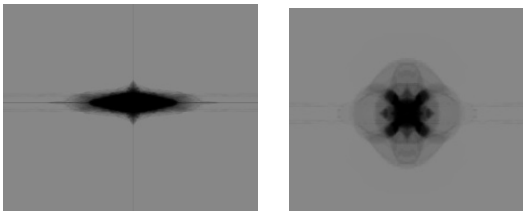

(a) UD (b) CP

Fig.7. Simulated delamination in the UD and CP laminates after impact (v = 400 m/s).

Table 5. Measured and predicted delamination area in the UD and CP laminates.

Laminate		UD		CP	
Velocity (m/s)		200	400	200	400
Delamination area (mm^2)	Measured	22.3	57.3	28.6	140.4
	Predicted	30	48	62	124

Table 6. Predicted delamination area in the CP laminates impacted at v = 400 m/s.

No.	1	2	3	4	5
Delamination area (mm^2)	124	115	124	128	116

and CP laminates. The shape of the delamination is a galaxy in the UD laminate and a circle in the CP laminate. Table 5 summarizes the measured and predicted delamination area in the UD and CP laminates for two impact velocities. It is demonstrated that the delamination area is greater at a larger impact velocity, and that the delamination area is greater in the CP laminate than in the UD laminate. Comparison between the measured data and the predictions is reasonable in both laminates.

Table 6 presents the predicted delamination area in the CP laminates at v = 400 m/s. The numbers in the table correspond to those in Table 4. It is surprising that the delamination area is hardly affected by lamina strength, although the interlaminar fracture toughness gives a little effect on the delamination area. Figure 8 depicts the tensile (red) and compressive (blue) failure of laminae in the CP laminates for (a) No. 2, (b) No. 1, and (c) No. 3. As the lamina strength becomes larger, the area of lamina failure becomes smaller. This result implies that the lamina strength affects the perforation limit rather than the degree of delamination. The reason for the limited effect of the interlaminar fracture toughness on the delamination is as follows. In the present analysis, only the values of G_i^C were varied while the values of the shear strength t_i^0 remain constant. This leads to the change in the critical displacement δ_i^C for complete delamination. However, for out-of-plane loading like impact,

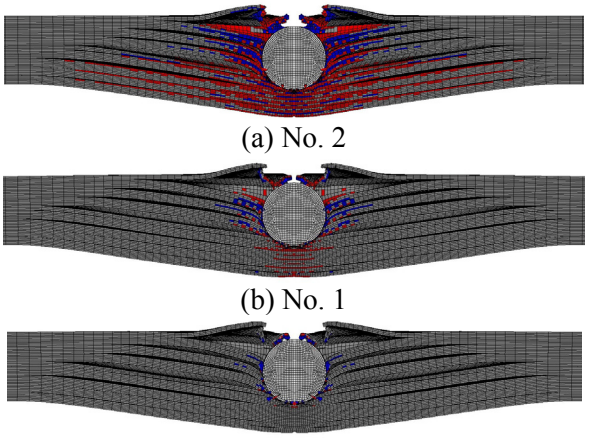

(a) No. 2

(b) No. 1

(c) No. 3

Fig. 8 Effect of σ_{1T} and σ_{1C} on failure of laminae in the CP laminates impacted at v = 400 m/s.

delamination is not remarkably affected by δ_i^C . If t_i^0 also varies with G_i^C , it is possible that the delamination area is largely changed. Therefore, the effect of t_i^0 on the delamination area will be investigated in the near future.

Conclusions

High-velocity impact damage in the UD and CP laminates is experimentally and numerically investigated. The simulation results were in qualitatively good agreement with the experiment results. Further investigation is required for clarifying the effects of material properties on damage evolution .

References

[1] K. Ogi, S. Yashiro, M. Takahashi, A. Yoshimura "Numerical and Experimental Characterization of High-Speed Impact Damage in CFRP Unidirectional and Cross-Ply Laminates". *Proceeding of ACCM-7*, 2010.

[2] P. H, Geubelle, J. S. Baylor "Impact-induced delamination of composites: a 2D simulation". *Composites Part B*, 1998.

[3] S. Yashiro, K. Ogi, "Fracture behavior in CFRP cross-ply laminates with initially cut fibers". *Composites Part A*, 2009.